J. Fluid Mech. (1987), *vol.* 181, *pp.* 77–97
Printed in Great Britain

Boundary layers in a sectioned centrifuge

By G. AMBERG
Department of Hydromechanics, Royal Institute of Technology, S-100 44 Stockholm, Sweden

AND H. P. GREENSPAN
Department of Mathematics, Massachusetts Institute of Technology, Cambridge, MA 02139, USA

(Received 15 May 1986 and in revised form 15 December 1986)

We consider the flow of a suspension in a rotating, cylindrical container with inclined endwalls and a dividing barrier that blocks any azimuthal motion around the axis. A boundary layer of clarified fluid appears when the influence of the Coriolis force is counteracted and although a bulk swirling motion is prevented by the meridional section, there is still an appreciable azimuthal flow in this thin purified-fluid layer. This flux produces an even more intense current on the leading side of the barrier (relative to the rotation direction) where the section meets the inclined wall.

1. Introduction

The time required for a mixture (in a jar, say) to settle is significantly decreased when the container is inclined with respect to gravity. Since the rate of production of pure fluid is proportional to the horizontal projection of the surface area between suspension and purified fluid, or suspension and sediment, inclination enhances settling by increasing this projected area, a phenomenon known as the Boycott effect. The fluid motion produced is characterized by a narrow, intense current of purified liquid that if heavier than the suspended particles falls along an upward-tilted wall (Probstein, Yung & Hicks 1977; Acrivos & Herbolzheimer 1979; and Schneider 1982).

Comparison of the bulk separation of mixtures in gravitational and centrifugal force fields illustrates many differences. In the simplest circumstances of gravitational settling of dilute mixtures that involves only vertical motion, regions of constant volume fraction α and velocity are separated by kinematic shocks (Kynch 1952). By contrast, centrifugal settling is also achieved by a squeezing process in addition to disengagement across interfaces, the physical variables are genuinely functions of time and position, and the velocity vectors have very large azimuthal components which affect separation through the conservation of angular momentum (Greenspan & Ungarish 1985*a*). Indeed, the vortex motion produced by a redistribution of angular momentum can even negate the influence of container geometry which is so important to the gravitational Boycott effect.

The analyses of the Boycott effect cited above show that the heavier pure-fluid layer on the upward-inclined wall is thin because of the need to balance buoyancy solely by shear forces. In rotating devices, the buoyancy force can be opposed by an equally large centrifugal pressure gradient caused by strong differential rotations between the zones of mixture and purified fluid. There is no physical necessity for a pure-fluid layer to remain thin, which it generally does not according to theoretical

prediction (Greenspan & Ungarish 1985*a*, *b*). It is concluded that centrifugal settling is essentially unaffected by the shape of a container whenever the Coriolis force is dominant. Moreover, geometrical enhancement of settling depends then on the extent to which this force can be negated. Although the pure-fluid boundary layer is properly regarded as a secondary occurrence in the descriptions of the gravitational Boycott effect, for centrifugal settling perceptions are reversed. The more appropriate generalization seems to be that unless the pure-fluid layer that forms in a rotating container remains thin, little or no geometrical enhancement of settling can occur. (An experimental test to confirm this prediction is described shortly.)

Perhaps the most important generalization about centrifugal separation crystallized from these studies is that while a large centrifugal acceleration is obviously important, the effects of the Coriolis force are mostly undesirable. Indeed, enhanced centrifugal separation depends on the manner and extent to which the Coriolis force is counteracted. The practical solution is to make shear forces important throughout the fluid domain by placing the endplates very close to each other in a disk-stack arrangement. This is probably an unrecognized design criteria, fortuitously satisfied in the quest to make the surface area available for settling as large as possible. Having reduced the influence of the Coriolis force in this way, the convective augmentation of settling, the Boycott effect, is made possible again (Bark, Johansson & Carlsson 1984; Amberg *et al.* 1986).

Another method to enhance centrifugal settling, proposed by Greenspan & Ungarish (1985*b*) is by the insertion of complete meridional barriers. Even a single barrier blocks the azimuthal fluid motion and thereby reduces the radial component of the Coriolis force. Moreover, the azimuthal pressure gradient sustained by the inserted wall causes a radially directed interior flow which could not otherwise exist. Vortex production is suppressed and the fluid motion is made to resemble the comparable flow in a purely gravitational field. The settling of a mixture in a sectioned cylinder with inclined endwalls is found to be enhanced essentially by the restoration of a Boycott effect. The analysis of this flow, which has been mostly kinematical to date, shows that in analogy with gravitational settling, a bulk mixture in which, for example, the fluid is heavier than the suspended particles is divided into three main regions separated by kinematic shocks: the clarified fluid where $\alpha = 0$ for $r > R(t)$; the suspension where $\alpha = \alpha_0(t)$ for $R(t) > r > S(t)$; and the sediment where $\alpha = \alpha_{\max}$, for $S(t) > r$. As the light particles settle towards the axis of rotation, a layer of heavy, clear fluid is formed on the inwardly inclined wall. This fluid is assumed to form a thin intense boundary-layer current and is rapidly transported out to the completely clarified region at $r > R$. It is the objective of this work to investigate the structure of this and any other purified layer that develops. To this end, we study the flow in a specific geometry that manifests the various boundary layers that are known to occur in rotating containers. The configuration, shown in figure 1, is a conical cylinder with a flat top, sectioned along a diameter by a single plate. An inner cylinder concentric with the rotation axis serves as a collection plate when required. Both compartments are assumed to be filled initially with a well-mixed suspension whose dispersed phase consists of small particles (or droplets) of approximately constant radius a, occupying the volume fraction α.

The dimensionless parameters that characterize the subsequent flow are

$$\epsilon = \frac{\rho_C - \rho_D}{\rho_C}, \quad \beta = \frac{2}{9}\frac{a^2}{(\nu_C/\Omega)}, \quad E = \frac{\mu}{\rho_C \Omega r_0^2},$$

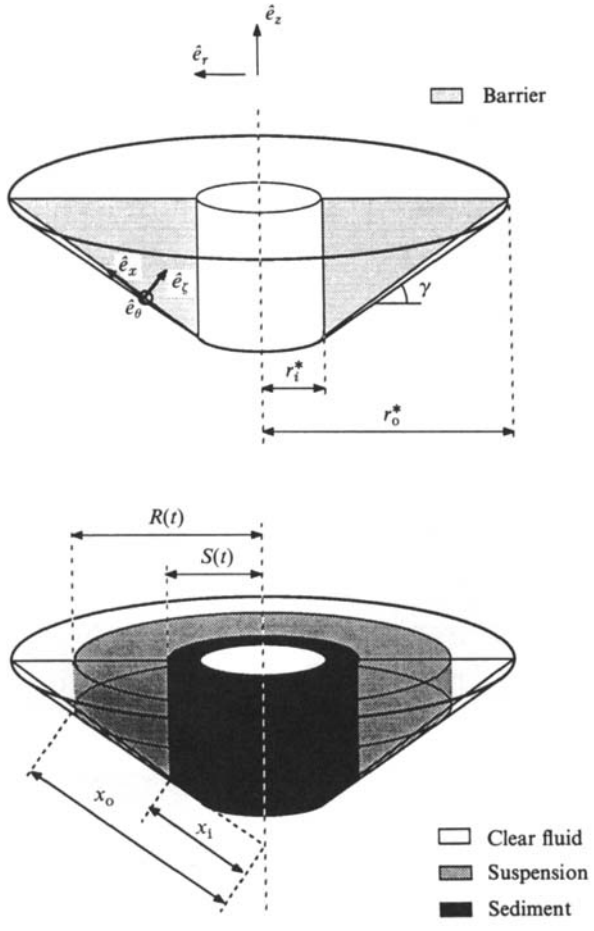

FIGURE 1. The geometry of the container. The shaded part is the barrier.

where μ is the effective viscosity coefficient of the mixture, ν_C is the kinematic viscosity of the fluid, r_o is the radius of the cylinder under consideration and Ω is the rotational speed of the container. (The averaged flow variables of the continuous and dispersed phases are denoted by subscripts C, D whereas an unsubscripted variable refers to the bulk mixture.) For purposes of experimental visualization and direct comparison with theory, the particles are taken as very slightly lighter than the suspending fluid, $0 < \epsilon \ll 1$. (The definition of ϵ here is the negative of that in earlier analyses.)

Parameter β, a modified Taylor number, measures the ratio of the particle size to the thickness of the Ekman layer, or equivalently the Coriolis force to the Stokes drag on a particle. Here, it is assumed that $\beta \ll 1$. We note that rapid rotation strongly affects the drag on a particle for β moderate or large. In particular, the velocity difference between particle (phase) and fluid (phase) is then no longer in the radial direction (Herron, Davis & Bretherton 1975; Greenspan 1983). Although this produces interesting effects as demonstrated by Schaflinger (1987), these are not considered here.

The Ekman number E, which measures the relative importance of viscous forces

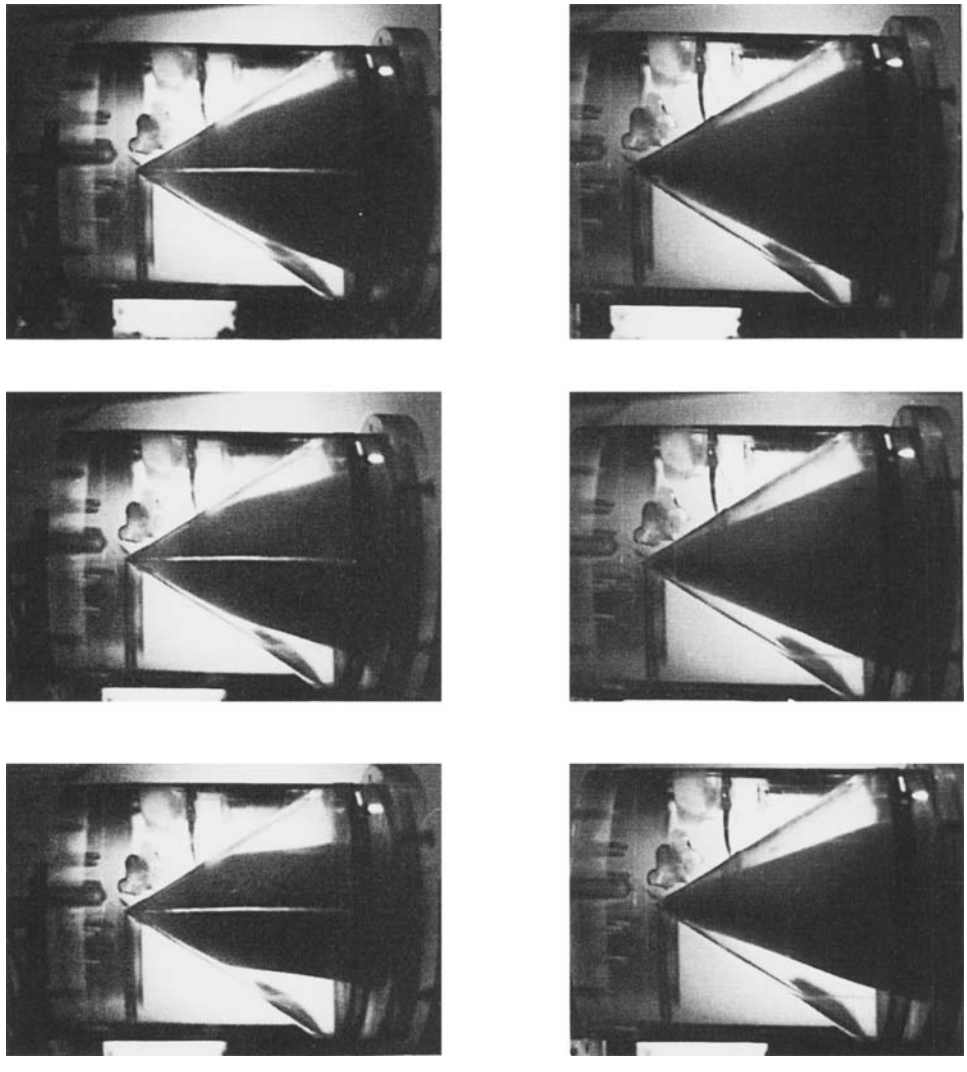

(a) (b)

FIGURE 2. (a) Photographs of settling in a cylindrically symmetric container with the dividing barrier. Pictures are taken at 1.0, 1.5, 2.0 min after the start of the experiment. (b) The same experiment but without the barrier in place. The barrier is viewed from the side and is visible as the light horizontal line in the centre of the container.

compared to the Coriolis acceleration is also assumed small. For the most part, however, the mixture is taken as fairly dilute and the volume fraction α, although still an $O(1)$ variable, is small.

As a necessary prelude to this theoretical study of centrifugal separation, a very qualitative experiment was undertaken to test at least the main predictions of Greenspan & Ungarish (1985*a*, *b*). Thus, bulk separation in a completely symmetric conical container should evince no thin purified layers of fluid and consequently no Boycott effect, if the ratio of the settling to spin-up times, $\lambda = E^{\frac{1}{2}}/\epsilon\beta$, is large. The insertion of a meridional barrier should, by nullifying the Coriolis force, produce once

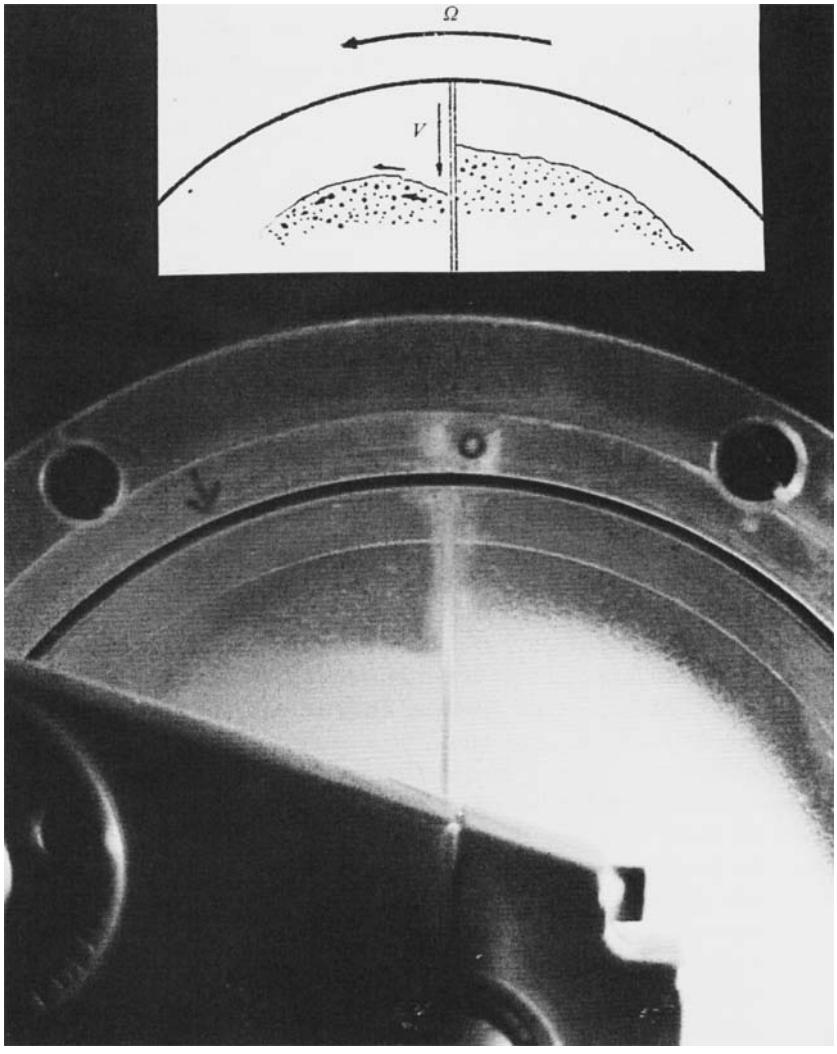

FIGURE 3. The flat lid of the container viewed along the axis of rotation during the experiment. The barrier is visible as the vertical line. The direction of rotation is such that the top rim moves to the left.

again a clarified boundary layer and augmented convective settling. (Although the analysis to support this requires small to moderate values of λ, this conclusion reflects a basic mechanism and seems valid for a much broader range.)

A container of the shape shown in figure 1 with radius of approximately 10 cm, was filled with a mixture of 40 % UCON 50-HB-5100 lubricant and 60 % water, the viscosity of which is $\nu_C = 0.75$ cm^2/s. A 12 % volume fraction of polystyrene beads with radii in the range 300 μm $< 2a <$ 425 μm constituted the dispersed phase. The container was mounted in a horizontal rig and rotated at $\Omega = 150$ rad/s. The values of the basic non-dimensional parameters are $E = 1.67 \times 10^{-5}$, $\beta = 0.015$, $\epsilon = 0.003$. Before each test the suspension was mixed by rocking the container back and forth until the concentration was deemed uniform. Observations and photography were made using a synchronized stroboscope. (Only a modest enhancement of settling, of

about 20%, is produced in this container; the operating conditions are chosen specifically for a study of boundary layers.)

Figure 2 shows the interface at 1, 1.5 and 2 min after the rotation was started for two cases. In case (*b*) the barrier has been removed, so that the container is completely axisymmetric. The region containing particles appears as the dark area. The interface between suspension and clear fluid is seen to be a cone concentric with the container but with an apex angle that continually decreases. There are no indications of thin clear boundary layers in good agreement with the theory. Since the radical bulk motion is small, the velocity of the interface is essentially equal to the slip velocity $\boldsymbol{q}_{\mathrm{R}}(=\boldsymbol{q}_{\mathrm{D}}-\boldsymbol{q}_{\mathrm{C}})$, which is proportional to r. This implies that the interface will be a collapsing cone, as observed.

In case (*a*) a meridional barrier has been inserted in the container. After 1.5 min the interface has the shape of a cone with the same apex angle as the container joined to a straight cylindrical front that extends to the baseplate of the container, and whose radius decreases with time. On the conical part of the interface, a thin clear boundary layer is visible as anticipated by physical arguments (and an analysis that is strictly valid for smaller values of λ than that of the experiment).

An unexpected observation is shown in figure 3, a photograph after one minute of the region where the baseplate of the cone meets the barrier. The direction of rotation is such that the rim is moving to the left in the picture. The flows on the two sides of the barrier are not the same and there are indications of intense currents of clear fluid during settling in the directions noted. These could originate in the peculiar dynamics of homogeneous rotating fluids in containers with no geostrophic contours (Greenspan 1968), or they could be a consequence of the settling process, as follows. In certain parametric ranges flow in the rotating pure-fluid boundary layer, unlike its gravitational counterpart, can have an azimuthal velocity component which transports mass to a still thinner and more intense radial jet located in the corner where the barrier meets the container wall. This current, emptying into the growing reservoir of purified fluid that forms in the evolution to the final state of completely separated components, would produce a flow pattern there that is consistent with the photograph. Better visualization techniques will be required to substantiate the existence of the corner layer. In any event, it seems not a trivial matter to subdue the Coriolis force completely.

2. The boundary layer on the conical wall

The theoretical formulation and analysis of bulk settling of a mixture in a rotating frame is given by Ishii (1975) and Greenspan & Ungarish (1985*b*). The equations of motion are written in terms of the non-dimensional variables obtained by scaling velocities by $\epsilon\beta\Omega r_{\mathrm{o}}$, (recall that $\epsilon=(\rho_{\mathrm{C}}-\rho_{\mathrm{D}})/\rho_{\mathrm{C}}>0$), lengths by r_{o}, the outer radius of the container, time by $(\epsilon\beta\Omega)^{-1}$ and density by ρ_{C}. The equations of continuity and momentum are then

$$\frac{\partial\alpha}{\partial t}+\nabla\cdot\left(\alpha\boldsymbol{q}+\frac{\alpha(1-\alpha)}{1-\epsilon\alpha}\boldsymbol{q}_{\mathrm{R}}\right)=0, \tag{2.1}$$

$$\nabla\cdot\boldsymbol{q}=\nabla\cdot\frac{\epsilon\alpha(1-\alpha)}{1-\epsilon\alpha}\boldsymbol{q}_{\mathrm{R}}. \tag{2.2}$$

$$(1-\epsilon\alpha)\left[2\hat{\boldsymbol{e}}_z\times\mathbf{q}+\epsilon\beta\left(\frac{\partial\boldsymbol{q}}{\partial t}+\tfrac{1}{2}\nabla\boldsymbol{q}\cdot\boldsymbol{q}+(\nabla\times\boldsymbol{q})\times\boldsymbol{q}\right)\right]$$
$$=-\frac{1}{\beta}\nabla P-\frac{\alpha r}{\beta}\hat{\boldsymbol{e}}_r+E[\tfrac{4}{3}\nabla\nabla\cdot\boldsymbol{q}-\nabla\times(\nabla\times\boldsymbol{q})]-\epsilon\beta\nabla\cdot\alpha(1-\alpha)\,\boldsymbol{q}_{\mathrm{R}}\boldsymbol{q}_{\mathrm{R}}, \tag{2.3}$$

where P is the reduced pressure. A simple law for the relative velocity is assumed as given by a modified Stokes scttling velocity in a centrifugal force field,

$$\boldsymbol{q}_{\mathrm{R}} = -f(\alpha)\, r\hat{\boldsymbol{e}}_r, \tag{2.4}$$

where $f(\alpha)$ accounts for the small-scale interaction between particles and fluid.

In order to study the thin layer of clear fluid that forms adjacent to the conical wall during the separation process, we assume that the flow has a boundary-layer character for $\epsilon, \beta, E \ll 1$. Boundary-layer coordinates x, θ, ζ, shown in figure 1 are defined by

$$\left.\begin{aligned} r &= x\cos\gamma - \delta\zeta\sin\gamma, \\ z &= x\sin\gamma + \delta\zeta\cos\gamma, \\ \theta &= \theta. \end{aligned}\right\} \tag{2.5}$$

The corresponding velocity components u, v, w in the (x, θ, ζ)-directions are

$$\left.\begin{aligned} u &= q_r\cos\gamma + q_z\sin\gamma, \\ v &= q_\theta, \\ w &= \frac{-q_r\sin\gamma + q_z\cos\gamma}{\delta}. \end{aligned}\right\} \tag{2.6}$$

In these expressions, δ is the boundary-layer thickness (which is yet to be determined) and γ is the inclination angle of the walls.

If terms negligible in the boundary-layer analysis are discarded, the momentum equations are

$$-2v\cos\gamma + \epsilon\beta\left(\frac{\mathrm{D}\boldsymbol{u}}{\mathrm{D}t}\right)\cdot\boldsymbol{e}_x = -\frac{1}{\beta}\Pi_x + \frac{\alpha_0-\alpha}{\beta}x\cos^2\gamma + \frac{E}{\delta^2}u_{\zeta\zeta}, \tag{2.7a}$$

$$2u\cos\gamma + \epsilon\beta\left(\frac{\mathrm{D}\boldsymbol{u}}{\mathrm{D}t}\right)\cdot\boldsymbol{e}_\theta = -\frac{1}{\beta}\frac{1}{x\cos\gamma}\Pi_\theta + \frac{E}{\delta^2}v_{\zeta\zeta}, \tag{2.7b}$$

$$2v\sin\gamma + \epsilon\beta\left(\frac{\mathrm{D}\boldsymbol{u}}{\mathrm{D}t}\right)\cdot\boldsymbol{e}_\zeta = -\frac{1}{\beta\delta}\Pi_\zeta - \frac{\alpha_0-\alpha}{\beta}x\cos\gamma\sin\gamma + \frac{E}{\delta}w_{\zeta\zeta}; \tag{2.7c}$$

likewise mass conservation is described by

$$(xu)_x + \frac{1}{\cos\gamma}v_\theta + xw_\zeta = 0. \tag{2.8}$$

Here a new pressure has been introduced:

$$\Pi = P + \tfrac{1}{2}\alpha_0(x\cos\gamma - \delta\zeta\sin\gamma)^2;$$

$\alpha_0(t)$ is the concentration in the interior, α is the actual concentration i.e. $\alpha = \alpha_0$ in the interior, $\alpha = 0$ in the purified fluid.

The magnitude of the velocities and the thickness of the boundary layer are estimated by requiring balance in momentum and continuity equations and an $O(1)$ net transport in the clear-fluid layer, i.e. $u\delta \approx 1$ or $v\delta \approx 1$. For ϵ, β, E small and $\alpha = O(1)$, consistent balances in different parameter regimes are found as given in table 1.

In the parameter range 1, the velocity in the clarified layer is essentially directed radially outwards. Since the effects of the Coriolis force are weak, the force balance in the clear layer is here similar to that in the non-rotating case (Acrivos & Herbolzheimer 1979). In scaling 2, the Coriolis force begins to be important and the velocity profile across the clear-fluid layer is that of two merging $E^{\frac{1}{2}}$ layers. The direction of the net flux is at an angle with the radial direction, approaching the

	u	v	δ
1. $E \gg \beta^2$	$(\beta E)^{-\frac{1}{3}}$	$(\beta E^2)^{\frac{1}{3}}$	$(\beta E)^{\frac{1}{3}}$
2. $E \approx \beta^2$	$E^{-\frac{1}{2}}$	$E^{-\frac{1}{2}}$	$E^{\frac{1}{2}}$
3. $\max(\beta^3, \epsilon\beta^2) \ll E \ll \beta^2$	E/β^3	$1/\beta$	β
4. $\epsilon \gg \beta$; $E \ll \epsilon\beta^2$	ϵ/β	$1/\beta$	β
5. $\epsilon \ll \beta$; $E \ll \beta^3$	1	$1/\beta$	β

TABLE 1. Magnitude of velocities and boundary-layer thickness for various parameter regimes

azimuthal direction if E is decreased further (with β fixed). In the ranges 3–5 the main force balance is geostrophic and the large buoyant term is balanced by the Coriolis force. The flow in the clear boundary layer is essentially in the azimuthal direction. (If ϵ is large, the force balance is between inertia, buoyancy and the Coriolis force which corresponds to the rotating version of the layer studied by Schneider (1982). This situation is not studied here.) It is of course very difficult in any real experiment to conform to the precise asymptotic requirements on the magnitudes of the parameters. However, the conditions for figure 2, would apply best to range 2, but possibly to range 5 as well.

From now on, we shall concentrate on parameter range 2 in which case the boundary-layer thickness of the clear-fluid layer is $\delta = E^{\frac{1}{2}}$, the same as that of the Ekman layers, the concentration within the suspension depends on time only, and order-one velocities may be defined by $(U, V, W) = E^{\frac{1}{2}}(u, v, w)$. The motion of the interface separating suspension and clarified fluid,

$$\zeta = s(x, \theta, \tau) \tag{2.9}$$

with $\tau = E^{-\frac{1}{2}}t$, is determined by the movement of the particles on this surface. Assuming $\epsilon, E^{\frac{1}{2}} \ll 1$, an equation for $s(x, \theta, \tau)$ may be derived as in Appendix A. The result is

$$s_\tau + \frac{1}{x}\frac{\partial}{\partial x}(xQ_x) + \frac{1}{x\cos\gamma}\frac{\partial}{\partial\theta}Q_\theta = x\cos\gamma\sin\gamma(1-\alpha)f(\alpha). \tag{2.10}$$

The bulk continuity equation (2.8) has been used here to replace the velocities by the non-dimensional fluxes of clear fluid in the x- and θ-directions:

$$Q_x = \int_0^s U\,\mathrm{d}\zeta, \quad Q_\theta = \int_0^s V\,\mathrm{d}\zeta. \tag{2.11}$$

The fast timescale τ implies that changes in the shape of the interface occur much more quickly than the overall settling process. As a consequence, the concentration $\alpha_0(t)$ which varies on the settling timescale is quasi-steady when analysing the motion and location of the interface. Likewise the shock that separates the suspension from the completely clarified region is steady on the τ-timescale.

Expressions for the flux functions Q_x, Q_θ are needed to compute $s(x, \theta, \tau)$. They are obtained from the momentum equations (2.7) upon neglecting small terms, using the rescaled variables and setting

$$\beta = bE^{\frac{1}{2}};$$

$$-2V\cos\gamma = -\frac{1}{b}\Pi_x + \frac{\alpha_0 - \alpha}{b}x\cos^2\gamma + U_{\zeta\zeta}, \tag{2.12a}$$

$$2U\cos\gamma = -\frac{1}{b}\frac{1}{x\cos\gamma}\Pi_\theta + V_{\zeta\zeta}, \tag{2.12b}$$

$$0 = -\frac{1}{b}\Pi_\zeta. \tag{2.12c}$$

The last equation implies that to lowest order, $\Pi = \Pi_{\text{interior}} = 0$. Moreover, since the clear-fluid layer is separated from the suspension by a sharp interface

$$\alpha = \begin{cases} 0, & \zeta < s(x,\theta,\tau) \\ \alpha_0, & \zeta > s(x,\theta,\tau). \end{cases}$$

Equations (2.12) are exactly those for an Ekman boundary layer. They may be solved for U, V using boundary conditions $U, V = 0$ at $\zeta = 0$, U, V, U_ζ, V_ζ continuous at $\zeta = s(x,\theta,\tau)$ and $U, V \to 0$ when $\zeta \to \infty$. The velocity profile is that of two merged $E^{\frac{1}{2}}$ layers in the clear fluid, driving one $E^{\frac{1}{2}}$ layer in the suspension, adjacent to the interface. The calculation of the flux functions U, V yields

$$\left.\begin{aligned} Q_x &= \alpha_0 \frac{x\cos\gamma}{2b}\,\mathrm{Re}\,(G(s;\gamma)), \\ Q_\theta &= \alpha_0 \frac{x\cos\gamma}{2b}\,\mathrm{Im}\,(G(s;\gamma)), \end{aligned}\right\} \tag{2.13}$$

where

$$G(s;\gamma) = -\mathrm{i}\left\{ s - \frac{1}{\kappa}\left[\frac{2(\cosh(\kappa s) - 1) + \dfrac{\sinh\kappa s}{k^{\frac{1}{2}}}}{\sinh\kappa s + \dfrac{\cosh\kappa s}{k^{\frac{1}{2}}}} \right] \right\}$$

and

$$\kappa = (2\mathrm{i}\cos\gamma)^{\frac{1}{2}}, \quad k = \mu_{\mathrm{m}}/\mu_{\mathrm{c}}.$$

The ratio k between the viscosities in the purified fluid and the suspension has been introduced here for completeness. To keep the analysis as simple as possible, k will in the following be taken to be 1, so that $f(\alpha) \approx 1$.

A physical requirement that has to be fulfilled on the barrier and at $x = x_{\mathrm{i}}$, where the sediment interface $r = S(t)$ touches the cone, is that there can be no normal flux of clear fluid at these locations. Therefore, $Q_x = 0$ at $x = x_{\mathrm{i}}$ and $Q_\theta = 0$ at the barrier. Inspection of the expression (2.14) for G shows that both of these are true only for $s = 0$, which is the only possible value of s on these boundaries. Furthermore, boundary conditions for hyperbolic equations such as (2.10) can only be specified on those parts of the boundary where the characteristic curves enter the domain. Equation (2.10) implies that s increases along characteristic curves. It follows from (2.14) that the characteristic velocity, which is zero for $s = 0$, is directed outwards and towards decreasing θ for small positive values of s. Thus, when s is integrated along a characteristic curve, starting on the boundary with $s = 0$, the curve bends towards increasing x and decreasing θ (opposite to the direction of rotation). Consequently, it is proper to apply the boundary condition $s = 0$ on the inner surface at $x = x_{\mathrm{i}}$ and on half the barrier at $\theta = \pi$, where such curves will be directed into the domain (see figure 4).

On the boundaries at $\theta = 0$ and $x = x_{\mathrm{o}}$, where characteristics leave the domain, additional analysis is required to explain how the mass balance is maintained. The situation is analogous to that common in asymptotic theory, when subcharacteristics leave the domain. Additional boundary layers are then required to account for the boundary conditions, which in this case are the conditions of continuity of mass flux

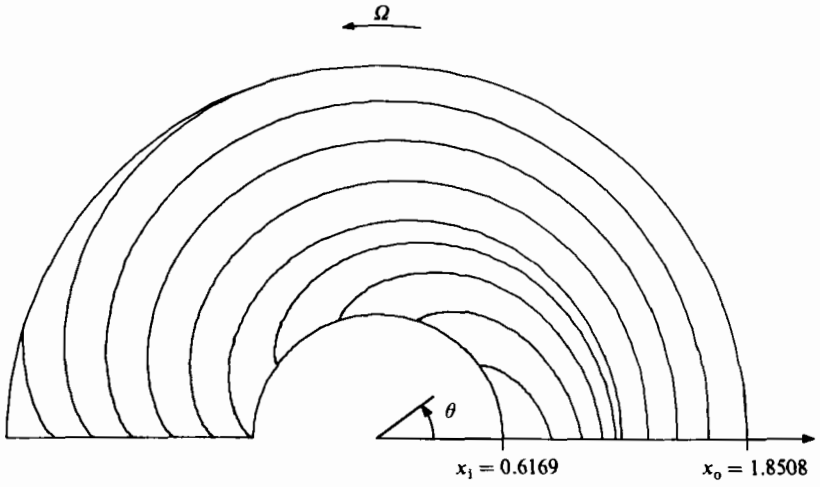

FIGURE 4. The characteristics of equation (2.10).

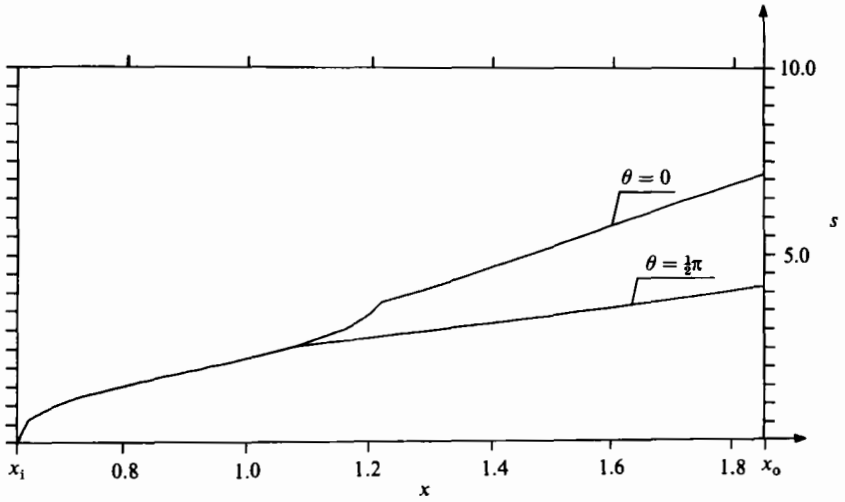

FIGURE 5. Thickness of the clear-fluid layer as function of x at two positions, $\theta = \frac{1}{2}\pi, 0$.

at $x = x_0$, and no net normal flux into the barrier at $\theta = 0$. The situation is not so dramatic at $x = x_0, \theta > 0$ where the outer cylindrical shock at $r = R$ meets the cone. The velocity of this shock is determined in accordance with the mass conservation law. However, at $\theta = 0$, the implication is that a net flux of clear fluid is forced into the barrier. Thus an additional layer must be present there in order to transport the clear fluid out to the completely clarified region $r > R$. This layer is discussed in detail in the next section.

As a specific illustration, let $\gamma = 1$, $b = 0.2$, $\alpha = 0.1$, $r_i = \frac{1}{3} \to x_i = r_i/\cos\gamma = 0.6169$, $r_0 = 1 \to x_0 = 1.8508$. Since $\alpha_0(t)$ and $R(t)$ are essentially steady on the τ-timescale, only the steady case need be examined. To compute $s(x, \theta)$, (2.10) is written in characteristic form and integrated numerically along characteristics all of which start on the boundary $x = x_i$ or $\theta = \pi$. Figure 4 shows some characteristic curves which are very much deflected from the radial direction. The thickness of the clear-fluid layer along two radii at $\theta = 0, \frac{1}{2}\pi$ is shown in figure 5.

The interface is independent of θ between the inner cylinder and the characteristic starting at $x = x_i, \theta = \pi$.

3. The corner boundary layer

As seen in the previous section, a flow of clear fluid is required that is directed outwards on the barrier at $\theta = 0$. For this reason, and on the basis of experimental indications, a reasonable hypothesis is that there is a current in a corner boundary layer, a region which is small in both the θ- and the ζ-directions. This jet is of interest because it may have serious effects on the separation process, perhaps by lessening the extent to which the Coriolis force can be counteracted, or by causing instabilities which remix the flow. These are as yet unresolved matters. The equations governing the motion in this layer will be derived and subsequently solved for an idealized case.

The new boundary-layer coordinates to be used are x, y, ζ, as shown in figure 6 and defined by

$$\left.\begin{aligned} r &= x\cos\gamma - \delta_2\zeta\sin\gamma, \\ z &= x\sin\gamma + \delta_2\zeta\cos\gamma, \end{aligned}\right\} \text{ at } \theta = 0,$$

$$y = \frac{x\cos\gamma\tan\theta}{\delta_1}.$$

This x-coordinate coincides at $\theta = 0$ with that used in the previous section. The lengthscales δ_1, δ_2, as well as the magnitudes of the velocity components remain to be determined.

The boundary-layer scaling of the equations requires a balance in the momentum and continuity equations, the ζ-component of the vorticity equation and an $O(1)$ transport, i.e. $u\delta_1\delta_2 \approx 1$. Working through the different possibilities, a consistent scaling is found to be

$$\left.\begin{aligned} \delta_1 &= E^{\frac{1}{3}}\left(\frac{\beta}{\alpha}\right)^{\frac{1}{2}}, \quad \delta_2 = \left(\frac{\beta}{\alpha}\right)^{\frac{1}{2}}, \quad u = \left(\frac{\alpha^2}{\beta^2 E}\right)^{\frac{1}{3}} U, \\ v &= \left(\frac{\alpha}{\beta}\right) V, \quad w = \left(\frac{\alpha^2}{\beta^2 E}\right)^{\frac{1}{3}} W, \quad \Pi = (\alpha\beta)^{\frac{1}{2}} P. \end{aligned}\right\} \tag{3.1}$$

The volume fraction α is represented in the scaling simply to illustrate the effect of a varied concentration; α is assumed to be larger than ϵ, β or $E^{\frac{1}{2}}$. The components of the velocity vector u, v, w in the (x, y, ζ)-directions are made non-dimensional as in §2; Π is the reduced pressure; U, V, W, P are the new scaled $O(1)$-variables. Note that $\delta_1 \ll \delta_2$, so that the corner region is larger in the ζ-direction than in the y-direction. Also $\delta_2 \gg \delta$, the thickness of the boundary layer on the conical plate. This scaling is consistent for

$$E < \frac{\beta}{\alpha}, \quad \epsilon < \min\left[\left(\frac{E^2}{\alpha\beta^2}\right)^{\frac{1}{3}}, \left(\frac{\beta}{\alpha^3}\right)^{\frac{1}{2}}, \left(\frac{E^4}{\beta\alpha^5}\right)^{\frac{1}{6}}\right].$$

Expressed in these $O(1)$-variables, the lowest-order boundary-layer equations are

$$-2V\cos\gamma = x\cos^2\gamma + U_{yy}, \tag{3.2a}$$

$$-2W\sin\gamma + 2U\cos\gamma = -P_y, \tag{3.2b}$$

$$2V\sin\gamma = -P_\zeta - x\cos\gamma\sin\gamma + W_{yy}, \tag{3.2c}$$

$$V_y + W_\zeta = 0. \tag{3.2d}$$

Note that U does not enter into the continuity equation and as seen from (3.1) u and w have the same magnitude. This means that apart from the rapid motion in the

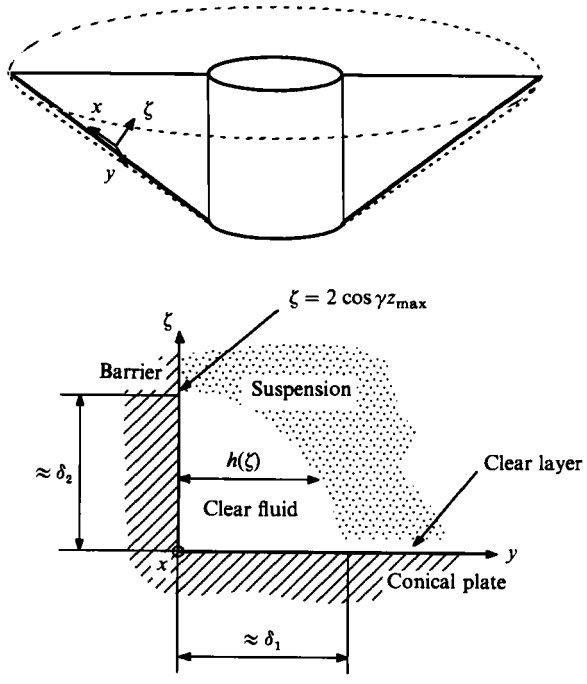

FIGURE 6. Definitions of coordinate system and symbols used to study the corner where the barrier meets the conical wall.

x-direction there is also a vortex-like motion in the (y, ζ)-plane. Thus a fluid particle does not move straight out in the x-direction but is more likely to travel along a spiral path. When the mass fluxes are integrated over the cross-section of the pure-fluid jet in the corner region, the lowest-order equation is

$$\int U \,\mathrm{d}y \,\mathrm{d}\zeta = F(x) = \int_{x_1}^{x} Q_\theta(s(\theta = 0, x)) \,\mathrm{d}x. \tag{3.3}$$

The right-hand side is obtained from (2.13).

The pressure can be eliminated and the x-dependence scaled out by introducing the following variables and definitions:

$$\zeta = 2z \cos\gamma, \quad U = x\eta \cos\gamma, \quad V = -\tfrac{1}{2}x\chi_z, \quad W = x \cos\gamma \chi_y. \tag{3.4}$$

The equations for χ, η are

$$\eta_{yy} - \chi_z = -\cos\gamma, \tag{3.5a}$$

$$\chi_{yyyy} + \eta_z = 0. \tag{3.5b}$$

These, except for the term $-\cos\gamma$, are the usual $E^{\frac{1}{3}}$ layer equations of rotating-fluid theory, see Greenspan (1968). The variable x has disappeared from the equations so that the x-dependence of the solution is determined by the mass-balance condition (3.3) which is

$$2\cos^2\gamma x \int \eta \,\mathrm{d}y \,\mathrm{d}z = F(x), \tag{3.6}$$

where the integration domain is over the cross-section of the jet.

The boundary conditions for the system (3.5) imposed at the solid boundaries are chosen to be

$$\eta = \chi = \chi_y = 0 \quad \text{at } y = 0, \tag{3.7}$$

$$\chi = 0 \quad \text{at } z = 0. \tag{3.8}$$

It is assumed that a thinner $E^{\frac{1}{2}}$ layer on the conical wall at $z = 0$ takes care of the no-slip condition there. Just as in ordinary $E^{\frac{1}{3}}$ layers, the Ekman suction is too weak to affect the lowest-order flow. Thus, only the requirement of no normal flow remains, $\chi = 0$. At $y = 0$ the conditions are those of no slip and no normal flow.

The remaining part of the boundary is the (unknown) interface between the clear liquid and suspension,

$$y = h(z).$$

The height of the corner, $z_{\max}(x)$, in figure 6 is the value for which $h(z_{\max}) = 0$. Equation (3.6) determines the x-dependence of $z_{\max}$, and thereby the x-dependence of η, χ.

The proper boundary conditions to use at $y = h(z)$ are the continuity of stress and velocity across the interface, which implies that $P, \eta, \eta_y, \chi, \chi_y, \chi_{yy}$ are continuous at $y = h(z)$. The requirement that $y = h(z)$ is a streamline provides one additional equation that determines $h(z)$:

$$\chi = 0 \quad \text{at } y = h(z).$$

With this set of boundary conditions the flow in the clear corner region will be coupled with that in the suspension in the vicinity of the corner. In order to solve (3.5), the flow outside the corner would thus have to be computed too. This is an effectively infinite region which makes a numerical solution considerably more difficult. An analytical treatment of the flow outside is of course complicated by the presence of a curved boundary.

Our objective at this point is not to determine the details of this flow exactly, but rather to make the existence of this corner layer seem probable, as well as the scales and magnitude estimates in (3.1). Of course, the qualitative features of the flow in this region are of interest. To this end, the problem is simplified by taking the boundary conditions at the interface $y = h(z)$ to be

$$\eta = \chi = \chi_y = 0, \quad x_{yyy} = \sin\gamma. \tag{3.9}$$

The first three of these boundary conditions imply that the suspension appears to the clear fluid in the corner region like a solid wall. This may be justified if the suspension is more viscous than the clear fluid, as is the case for high concentrations. If $k = \mu_{\mathrm{m}}/\mu_{\mathrm{c}} \gg 1$, it is possible to derive estimates of the magnitudes of the values of the flow variables on the interface which are $U \approx k^{-\frac{2}{3}}$, $V \approx k^{-\frac{1}{3}}$, $W \approx k^{-\frac{2}{3}}$ and $P \approx k^{-\frac{1}{3}}$. The velocities and also the pressure should then vanish to lowest order on the interface. The last of the four conditions (3.9) may be seen from (3.2*b*) and (3.2*c*) to be equivalent to $P = \text{const}$ on $y = h(z)$. Although the assumption of a very viscous suspension may not be particularly good at concentrations of say, 10 % corresponding to the experiment, it should at least serve as a physically reasonable model problem that shows the qualitative features of the corner flow. To make sure that the scaling rules in (3.1) are valid, it is also important to check that it is indeed possible to solve the equations for the corner region.

We turn now to the solution of (3.5) subject to boundary conditions (3.7)–(3.9). The essential simplification introduced by using the boundary condition (3.9) is that

the domain becomes finite. The equations (3.5) are linear, but the problem is still highly nonlinear because the shape of the interface $h(z)$ is unknown. Note that (3.7), (3.9) provide seven boundary conditions on $y = 0, \delta(z)$. Given a fixed $h(z)$, six of these specify η, χ uniquely and the seventh is used as an equation for $h(z)$.

An analytical approach is based on a change of variables

$$\mu = \frac{y}{h(z)}, \quad \xi = h(z) \tag{3.10}$$

and series solutions of the form

$$\chi(x,y,z) = \chi_0(\mu)\,\xi^{a_0} + \chi_1(\mu)\,\xi^{a_1} + \ldots, \tag{3.11a}$$

$$\eta(x,y,z) = \eta_0(\mu)\,\xi^{b_0} + \eta_1(\mu)\,\xi^{b_1} + \ldots, \tag{3.11b}$$

$$z = z_{\max} + C_0\,\xi^{d_0} + C_1\,\xi^{d_1} + \ldots. \tag{3.11c}$$

The last expression is an expansion of $z(\xi)$ in powers of ξ, the inverse of $\xi = h(z)$. These sums are meant to extend over all powers a_k, b_k, d_k that are consistent with the equations and the boundary conditions.

The lowest-order equations for χ_0, η_0 are obtained by introducing (3.11) into (3.5), collecting terms containing ξ raised to powers a_0, b_0 or d_0. Consistency then requires that $a_0 = 3, b_0 = 2, d_0 = 3$, in which case the resulting equations for χ_0, η_0 are

$$3C_0\,\eta_0'' - 3\chi_0 + \mu\chi_0' = -3C_0\cos\gamma, \tag{3.12a}$$

$$3C_0\,\chi'''' + 2\eta_0 - \mu\eta_0' = 0. \tag{3.12b}$$

The corresponding boundary conditions are

$$\left.\begin{aligned} \chi_0 = \chi_0' = \eta_0 = 0, \quad & \text{at } \mu = 0, 1; \\ \chi_0''' = \sin\gamma \quad & \text{at } \mu = 1. \end{aligned}\right\} \tag{3.13}$$

Six of the seven boundary conditions at $\mu = 0, 1$ are needed to determine ξ_0, η_0 as functions of μ and C_0; the seventh condition is used to find the value of C_0. The differential equations are regular and may thus be solved by a power series expansion

$$\eta_0 = \Sigma\, b_n \mu^n, \quad \chi_0 = \Sigma\, c_n \mu^n.$$

The results of inserting these sums in the equations and working out the first powers are

$$\eta_0(\mu) = \tfrac{1}{2}\cos\gamma\,\mu(1-\mu) + O(\mu^4), \tag{3.14a}$$

$$\chi_0(\mu) = -\frac{\cos\gamma}{720C_0}\mu^2(\mu^3 - 3\mu + 2) + O(\mu^8), \tag{3.14b}$$

$$C_0 = -\frac{7}{120\tan\gamma}. \tag{3.14c}$$

The corresponding expressions for η, χ, h as functions of y, z are

$$\eta = \tfrac{1}{2}\cos\gamma\, y(h-y), \tag{3.15a}$$

$$\chi = -\frac{\cos\gamma}{240}h'y^2(2h^3 - 3h^2y + y^3), \tag{3.15b}$$

$$h = (\tfrac{120}{7}\tan\gamma(z_{\max} - z))^{\frac{1}{3}}. \tag{3.15c}$$

These expressions satisfy (3.5) approximately and the boundary conditions on $y = 0$ and at $y = h(z)$. Figure 7 (*a*) shows level curves of χ according to (3.15). Obviously,

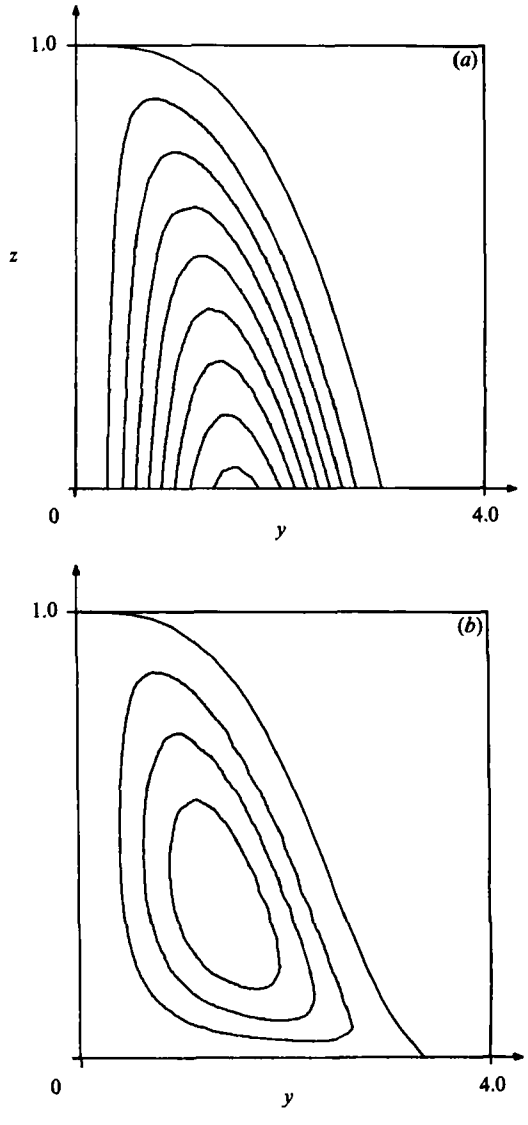

FIGURE 7. (*a*) Streamlines according to the approximation solution (3.15). The stream function χ is 0 at the wall and the clear-suspension interface. On the streamlines, it has the values $\chi = 0.01, 0.02, \ldots, 0.08$. (*b*) Numerically computed streamlines. The stream function χ has the values $\chi = 0, 0.01, 0.02, 0.03$ on the streamlines. It is 0 at the walls and on the clear-suspension interface.

the condition $\chi = 0$ on $z = 0$ is violated but, as will be seen later, these expressions are fair approximations of the solution away from the lower boundary. The boundary condition at $z = 0$ can be met by calculating the higher-power terms containing η_k, χ_k in (3.11) and the details of this analysis are given in Appendix B.

The problem was also solved by a direct numerical method. The system (3.5) was discretized using second-order-accurate finite differences and the solution was computed iteratively in two steps:

(i) the linear problem is solved, using $h(z)$ from the last iteration, without imposing the boundary condition $\chi_{yyy} = \sin\gamma$ at $y = h(z)$;

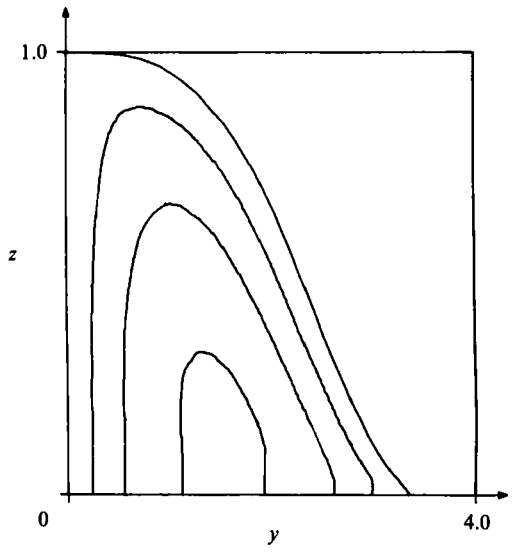

FIGURE 8. Level curves of η, the velocity in the x-direction. η is 0 on the wall and the clear-suspension interface. On the level curves it has the value $\eta = 0.15, 0.30, 0.45$.

(ii) $h(z)$ is corrected so that the error in $\chi_{yyy} = \sin\gamma$ is decreased along $y = h(z)$.

The expressions (3.15) are used as initial approximations and the iteration is continued until the absolute value of $\chi_{yyy} - \sin\gamma$ decreases by four or five orders of magnitude along the curved boundary. Step (ii) is executed with an approximate Newton–Raphson method; the correction $\mathrm{d}h_j$ to h_j, the value of $h(z)$ at the jth point $z = z_j$, is solved from the linear set of equations

$$-F_i = \sum_j \frac{\partial F_i}{\partial h_j} \mathrm{d}h_j, \tag{3.16}$$

where

$$F_i(h_j) = \chi_{yyy}(z_i, y = h_j) - \sin\gamma.$$

Here the left-hand side is the current numerically computed value of $F = \chi_{yyy} - \sin\gamma$, while the gradients in the right-hand side are calculated from the current values of h_j using (3.15).

Figure 7 (*b*) shows streamlines in a (y, z)-plane for the numerically computed χ, for the parameter values $\gamma = 1$ and $z_{\max} = 1$. A comparison with the approximate solution figure 7 (*a*) shows that the two are in fair agreement away from the $z = 0$ boundary, at least for $z > 0.5$. Level curves for η, shown in figure 8 indicate η is approximately a parabolic function of y at all z-values. The interfaces in figure 7 coincide with the streamline $\chi = 0$; a comparison of the two, figure 9, shows that the difference is fairly small, even near $z = 0$. The numerically computed interface which is slightly flatter than the analytical approximation does not seem to have the exact similarity shape $(z_{\max} - z)^{\frac{1}{3}}$, since it changes curvature and bends outwards near $z = 0$. Higher-order terms may rectify the discrepancy.

Finally the flow in the corner is matched to the solution on the conical plate. This is done by calculating the volume flux $F(x)$ of clear fluid required in the corner to take care of the inflow from the boundary layer on the conical wall as expressed by (3.3). The right-hand side of (3.3) was computed from the data presented in figure 5 and the non-dimensional flux $F(x)$ obtained in this way is shown in figure 10 (*a*). The

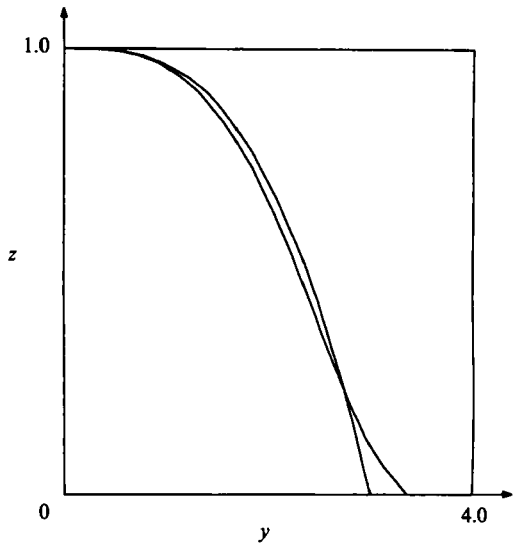

FIGURE 9. Comparison of the numerical and analytical solutions for the clear-suspension interface, $y = h(\zeta)$.

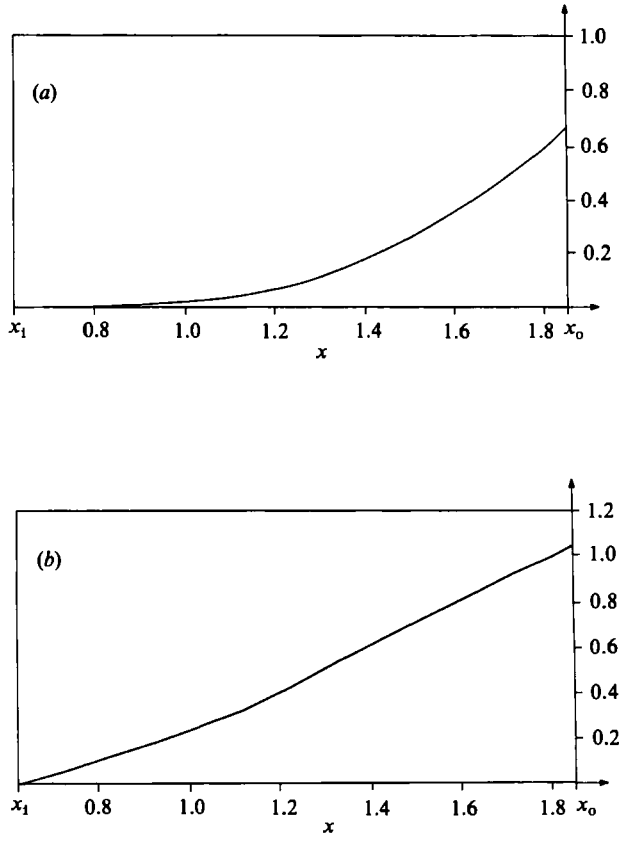

FIGURE 10. (*a*) The non-dimensional flux of clear fluid $F(x)$ that is required in the corner layer. (*b*) The non-dimensional height $z_{\max}$ of the clear corner jet as a function of x.

integral on the left-hand side of (3.6) determines $z_{max}(x)$. The analysis of the corner boundary layer in §3 assumes that $k = \mu_m/\mu_c \gg 1$ while, in the calculations leading to figure 10(*a*), k was taken equal to one. However the corner layer was also analysed for the case $k \ll 1$. It was found that, for the same value of z_{max}, the flux carried by the corner layer was almost the same in the two cases, about 7 % less in the $k \ll 1$ case than in the $k \gg 1$. It thus seems reasonable to assume that the dependence of the flux on k is weak and, in order to determine the x-dependence of z_{max}, the solution in §3 and figure 10(*a*) may be used. The result is shown in figure 10(*b*). Since η, ξ, h depend on x only through their dependence on $z_{max}(x)$, they are now completely specified.

4. Conclusions

A method for enhancing centrifugal separation by a modification of centrifuge geometry was examined by Greenspan & Ungarish (1985*b*). They showed that, unlike gravitational settlers, widely spaced, inclined end caps in a rotating cylindrical container do not increase separative performances *unless* the swirling motion is blocked by a meridional barrier. In this way the Coriolis force can be counteracted, as it is by viscous shear in the conventional arrangement of a closely spaced disk stack. A qualitative experiment reported here was in reasonable agreement with the theory. No Boycott effect was observed in the completely axisymmetric container with one flat and one conical end plate in that there were no thin clarified boundary layers on the inclined lid. However, with the insertion of the meridional barrier, the flow was radically altered and a boundary-layer flow, similar to that in non-rotating inclined settling, was then observed.

The scales relevant for the clarified boundary layer on the inclined lid and an equation for the thickness of the clear fluid layer were derived. The shape of the clear fluid–suspension interface which is quasi-steady on the settling timescale was computed for a special case. There is a considerable azimuthal flux in this boundary layer, driven via the Coriolis acceleration by the large radial buoyant force in the clarified layer.

This azimuthal flow implies that a corner layer is required where the meridional barrier and the conical end plate meet in order to transport the clear fluid in the main boundary layer out along the section to the completely clarified region. The corner current appears only on the front side of the barrier, i.e. that side which corresponds to an increasing azimuthal angle. On entering the boundary layer, the angular momentum of an element of purified fluid decreases so that it acquires a retrograde azimuthal velocity relative to the container. Upon meeting the barrier, the azimuthal motion of the fluid is effectively stopped and the bouyancy force throws it radially outwards into the region of purified liquid $r > R(t)$. There buoyancy forces are absent and a more conventional rotating source–sink flow redistributes the fluid so that overall mass balance is maintained.

The problem for the flow in the corner is fully nonlinear since the shape of the boundary between clarified fluid and suspension is unknown. It was solved in a slightly idealized case and the structure of the corner jet determined both analytically and numerically. Experimental work to verify results is contemplated.

We are grateful to Professor Fritz Bark and Dr Marius Ungarish for valuable comments and criticism. This research was partially supported by the National Science Foundation, Grant Number MCS-8213987.

Appendix A

The position of the interface between clear fluid and suspension is denoted by

$$\zeta = s(x, \theta, \tau). \tag{A 1}$$

The coordinates x, θ, ζ are defined in (2.5); τ is a fast time variable defined by $\tau = E^{-\frac{1}{2}}t$. If (A 1) is differentiated with respect to t we obtain

$$\frac{\mathrm{d}\zeta}{\mathrm{d}t} = \frac{\partial s}{\partial x}\frac{\mathrm{d}x}{\mathrm{d}t} + \frac{\partial s}{\partial \theta}\frac{\mathrm{d}\theta}{\mathrm{d}t} + E^{-\frac{1}{2}}\frac{\partial s}{\partial \tau}. \tag{A 2}$$

Since the motion of the interface is determined by the motion of the particles located on the interface, $\mathrm{d}x/\mathrm{d}t$, $r\,\mathrm{d}\theta/\mathrm{d}t$ and $\mathrm{d}\zeta/\mathrm{d}t$ may now be identified with the velocities of the dispersed particles on the interface, u_{D}, v_{D} and w_{D}. Furthermore, the particle velocities are related to the bulk velocities u, v, w by

$$\boldsymbol{q}_{\mathrm{D}} = \boldsymbol{q} + \frac{1-\alpha}{1+\epsilon\alpha}\boldsymbol{q}_{\mathrm{R}}.$$

Using this, the definition of $\boldsymbol{q}_{\mathrm{R}}$ in (2.4), and the variable transformation (2.6), the particle velocities may be written as

$$\left.\begin{aligned} u_{\mathrm{D}} &= \frac{\mathrm{d}x}{\mathrm{d}t} = u - (1-\alpha)f(\alpha)\,x\cos^2\gamma, \\ v_{\mathrm{D}} &= \frac{r\,\mathrm{d}\theta}{\mathrm{d}t} = v, \\ w_{\mathrm{D}} &= \frac{\mathrm{d}\zeta}{\mathrm{d}t} = w + E^{-\frac{1}{2}}(1-\alpha)f(\alpha)\,x\sin\gamma\cos\gamma. \end{aligned}\right\} \tag{A 3}$$

The assumption $\epsilon \ll 1$ has been used, and small terms have been neglected. The introduction of (A 3) into (A 2) yields

$$E^{-\frac{1}{2}}(1-\alpha)f(\alpha)\,x\sin\gamma\cos\gamma = E^{-\frac{1}{2}}\frac{\partial s}{\partial \tau} + \frac{\partial s}{\partial x}(u-(1-\alpha)f(\alpha)\,x\cos^2\gamma) + \frac{\partial s}{\partial \theta}\frac{v}{r} - w. \tag{A 4}$$

Since the velocities u, v, w are to be evaluated at the interface $\zeta = s(x, \theta, \tau)$, the continuity equation (2.8) allows some of the terms on the right-hand side of (A 4) to be rewritten as

$$\frac{\partial s}{\partial x}u + \frac{\partial s}{\partial \theta}\frac{v}{x\cos\gamma} - w = \frac{1}{x}\frac{\partial}{\partial x}\left(x\int_0^s u\,\mathrm{d}\zeta\right) + \frac{1}{x\cos\gamma}\frac{\partial}{\partial \theta}\left(\int_0^s v\,\mathrm{d}\zeta\right). \tag{A 5}$$

The substitution of this expression into (A 4), with non-dimensional fluxes defined by

$$Q_x = E^{\frac{1}{2}}\int_0^s u\,\mathrm{d}\zeta, \quad Q_\theta = E^{\frac{1}{2}}\int_0^s v\,\mathrm{d}\zeta. \tag{A 6}$$

yields, upon neglecting low-order terms,

$$\frac{\partial s}{\partial \tau} + \frac{1}{x}\frac{\partial}{\partial x}(xQ_x) + \frac{1}{x\cos\gamma}\frac{\partial}{\partial \theta}Q_\theta = (1-\alpha)f(\alpha)\,x\sin\gamma\cos\gamma. \tag{A 7}$$

This is the result cited in (2.10).

Appendix B

To obtain the higher-order terms of the series solution to (3.5) as formulated in (3.10), (3.11) *et seq.*, the expansions are substituted into these equations and terms containing ξ raised to powers containing exactly one of a, b, or d, are collected. To obtain the next-order equations, (3.11) is inserted into (3.5) and terms containing ξ raised to powers containing exactly one of a_1, b_1 or d_1 are collected. Consistency now requires that all these powers are in fact the same. It follows that

$$b_1 = a_1 - 1, \quad d_1 = a_1,$$

but a_1 is not determined. The system of equations for η_1, χ_1, C_1 and a_1 is

$$3C_0\eta_1'' - a_1\chi_1 + \mu\chi_1' = -C_1 a_1(\cos\gamma + \eta_0''), \tag{B 1}$$

$$3C_0\chi_1'''' + (a_1 - 1)\eta_1 - \mu\eta_1' = -C_1 a_1 \chi_0'''' \tag{B 2}$$

into boundary conditions

$$\left.\begin{aligned} \chi_1 = \chi_1' = \eta_1 = 0 \quad & \text{at } \mu = 0, 1, \\ \chi_1''' = 0 \quad & \text{at } \mu = 1. \end{aligned}\right\} \tag{B 3}$$

Note that the right-hand sides of (B 1) and (B 2) are both proportional to C_1 and that the boundary conditions (B 3) are homogeneous. Thus η_1, χ_1 are also proportional to C_1 and the value of C_1 cannot be determined by one of the boundary conditions in the way that C_0 was. In fact C_1 is easily scaled out from the equations. Instead the value of the exponent a_1 which is independent of C_1 is obtained from applying the last of the boundary conditions (B 3). Thus the solution is completely specified to this order, except for the constant C_1. The consistency of the scheme requires that the powers in the sums (3.11) are indeed increasing, and specifically that $a_1 > a_0 = 3$. Equations (B 1) and (B 2) were solved approximately by the method leading to (3.14) and, by using slightly more accurate forms of η_0, η_1 and χ_0, χ_1, the value of a_1 was determined to be 9.0589 for a case with $\gamma = 1$.

In this manner, the development (3.11) to higher powers should yield a series solutions for χ as

$$\chi = \chi_0(\mu)\,\xi^{a_0} + \sum_k C_k X_k(\mu)\,\xi^{a_k},$$

where $\chi_k = C_k X_k$. The coefficients C_k can then be determined to satisfy the remaining boundary conditions, $\chi = 0$ at $z = 0$.

REFERENCES

Acrivos, A. & Herbolzheimer, E. 1979 Enhanced sedimentation in settling tanks with inclined walls. *J. Fluid Mech.* **92**, 435–457.

Amberg, G., Dahlkild, A. A., Bark, F. H. & Henningson, D. S. 1986 On time-dependent settling of a dilute suspension in a rotating conical channel. *J. Fluid Mech.* **166**, 473–502.

Bark, F. H., Johansson, A. V. & Carlsson, C.-G. 1984 On a class of rotating viscous flows occurring in separation technology. *J. Méc. Theor. Appl.* **3**, 861.

Greenspan, H. P. 1968 *The Theory of Rotating Fluids.* Cambridge University Press.

Greenspan, H. P. 1983 On centrifugal separation of a mixture. *J. Fluid Mech.* **127**, 91–101.

Greenspan, H. P. & Ungarish, M. 1985*a* On the centrifugal separation of a bulk mixture. *Intl J. Multiphase Flow* **11**, 825–835.

Greenspan, H. P. & Ungarish, M. 1985*b* On the enhancement of centrifugal separation. *J. Fluid Mech.* **157**, 359–373.

HERRON, I. D., DAVIS, H. & BRETHERTON, F. P. 1975 On the sedimentation of a sphere in a centrifuge. *J. Fluid Mech.* **68**, 209–234.

ISHII, M. 1975 *Thermo-Fluid Dynamic Theory of Two-Phase Flow.* Eyrolles.

KYNCH, G. J. 1952 A theory of sedimentation. *Trans. Faraday Soc.* **48**, 166–176.

PROBSTEIN, R. F., YUNG, D. & HICKS, R. E. 1977 A model for Lamella settlers. *Physical Separations: Proc. Conf. Engineering Foundation, New York, 30 October to 4 November 1977*, pp. 53–92.

SCHAFLINGER, U. 1987 Sedimentation in cylindrical centrifuges with compartments. *Ing. Arch.* (submitted).

SCHNEIDER, W. 1982 Kinematic-wave theory of sedimentation beneath inclined walls. *J. Fluid Mech.* **120**, 323–346.